International Journal for Modern Trends in Science and Technology, 9(03): 186-194, 2023

ISSN: 2455-3778 online
DOI: https://doi.org/10.46501/IJMTST0903028
Available online at: http://www.ijmtst.com/vol9issue03.html

A Single-Stage Control Strategy with Energy Management for PV/Battery Hybrid Systems

P.Ganga Bhavani, KVVR.Satyamurthy, Vina Kumari, Dr.D.Ravi Kishore

Department of Electrical Engineering, Godavari Institute of Engineering and Technology(A), Rajahmundry, A.P, India.

To Cite this Article
P.Ganga Bhavani, KVVR.Satyamurthy, Vina Kumari and Dr.D.Ravi Kishore. A Single-Stage Control Strategy with Energy Management for PV/Battery Hybrid Systems. International Journal for Modern Trends in Science and Technology 2022, 9(03), pp. 186-194. https://doi.org/10.46501/IJMTST0903028

Article Info
Received: 26 February 2023; Accepted: 15 March 2023; Published: 18 March 2023

ABSTRACT

Proportional–integral (PI) energy strategy (EMS) and microgrid operations are presented to function independently of the grid in this study report. the photovoltaic system It provides just what is required. To get the most out of the PV electricity, it employs power tracking in addition to DC/DC and DC/AC converters. Parameters like charge status are within the controller's purview in traditional proportional-integral (PI) control (SOC). The maximum power-point tracking (MPPT) advantage for power distribution and battery charging/discharging has to be considered in the three distinct situations. The suggested power generating system's performance under different operating circumstances and with the enabled control methods is simulated in Matlab/Simulink.

KEYWORDS— Induction motor drive; electric vehicle application; DC microgrid; energy management; hybrid power system; energy efficiency

1. INTRODUCTION

Microgrids, or distributed energy systems (DES), are a kind of energy distribution network that use batteries and supercapacitors to maintain a constant voltage and current in the grid while storing energy for later use. Together and individually for tiny regions, all of these components are employed as a single grid [6,7]. Microgrids may be thought of as a network of grids, as seen in Figure 1. employing a utility grid for power distribution has various problems, such as loss of energy in transmission, air pollution from the producing phases, and global warming owing to traditional sources To address these problems, microgrids may be implemented. Microgrids may lower the loss, reduce CO2 emissions, particularly when employing renewable energy for power production. There are a few positives, too, such as lowering the danger of outages, selling electricity to national networks or net metering. Use of renewable energy sources, in addition to storage components, results in the highest possible system efficiency. [9–11] The microgrid is regulated by an EM (MGR). it incorporates several strategies to increase performance The proportional-integral-derivative (PID) control, the proportional-integral (PI) control, and the analogous decoupling techniques are the types of controls being discussed (EMC)

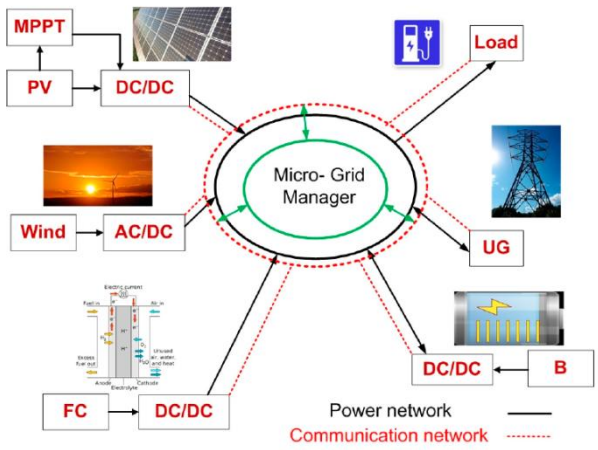

Figure 1. Configuration of DC microgrid

Two types of microgrids, ACMG and DCMG, were addressed by Manoj et al. [13]. (DCMG). Superior efficiency, simplified DC bus connectivity, and increased device dependabilities are just a few of the ways in which the DCMG excels above its ACMG counterpart. Power exchange fluctuations, power variation between the storage system and the power sources, and rapid changes in the DC bus load were all verified to have an impact on power disturbances in DCMGs.

A MG system powered by wind and hydropower was created by Ravichandrudu et al. [14], which offers the dual benefit of lowering transmission losses and helping the environment.

2. MODEL OF PV CELL

When light is shined on the solar cell, it will generate voltage. They are shown in the Fig1

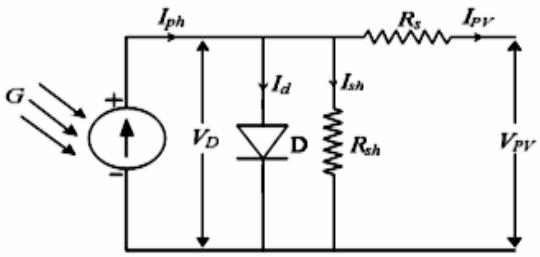

Fig1: Modeling a PV cell mathematically

The following set of equations (1) through (6) is used to model a PV panel.The current from PV panel is given by

$$I_{pv} = I_{ph} - I_d - I_{sh} \qquad (1)$$

The Photo generated current is given by

$$Iph = G \times (Isc + (K_i \times (T_{op} - T_{ref}))) \qquad (2)$$

The diode current is given by

$$I_d = I_s \times (e^{q \times (\frac{V_{pv} + I_{pv} \times Rs}{Ns \times n \times V_t \times c})} - 1) \qquad (3)$$

The saturation current is given by

$$I_s = I_{rs} \times \left(\frac{T_{op}}{T_{ref}}\right) \times e^{\left(\frac{1}{T_{op}} - \frac{1}{T_{ref}}\right) \times \left(\frac{E_g \times q}{K \times n}\right)} \qquad (4)$$

Where the reverse saturation current is given by

$$I_{rs} = \frac{I_{sc}}{e^{\left(\frac{q \times V_{oc}}{K \times C \times T_{op} \times n}\right)} - 1} \qquad (5)$$

Where E_g = Energy Gap of PV material =1.12ev

The shunt current is given by

$$I_{sh} = \left(\frac{V_{pv} + (I_{pv} \times R_s)}{R_{sh}}\right) \qquad (6)$$

Using real-world electrical data from PV panels, we can determine the optimal number of cells to connect into an array. Table 1. The modelled PV panel has accurate I-V and P-V characteristics that match the specifications given by the manufacturer.

3. Energy Management System in DC Microgrid

The following diagram depicts the PV/battery distributed system. This three-port gadget couples a photovoltaic source to a direct current load. To maintain consistent battery power, it may be charged or drained to act as a buffer. Figure 2 depicts how the DC-to-V and V-to-B buck/boost converters in the power-density system use an integrated topology.

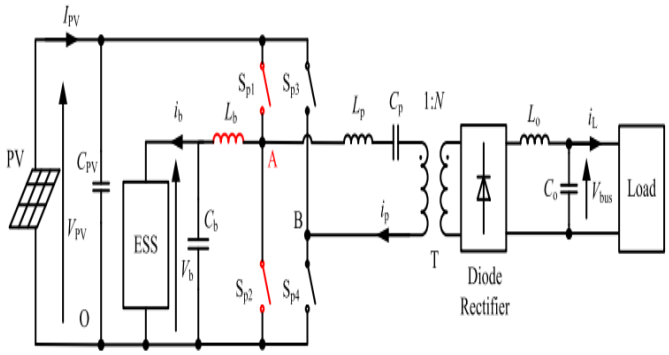

FIGURE 3.2. The proposed PV/battery hybrid distributed power generation system.

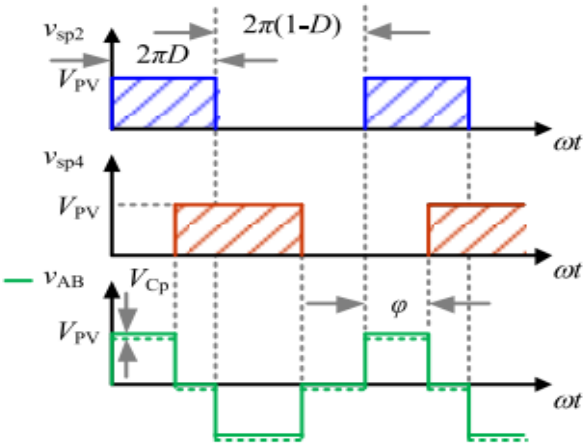

FIGURE 3.3. The phase shiftangle' and the duty cycle D form the modulation strategy of the full bridge.

As can be seen in Fig. 3, this bridge operates with an improved phase shift modulation. Both legs of the major bridge's leg-to-limb switch are asymmetrical. As an added bonus, switch A on the right leg 1's duty cycle may be lowered while all other legs cycle at 50%.

Specifically, Fig. 2 draws attention to the main side of the HF transformer's bidirectionalium-boost converter. The battery and capacitor in leg A are unnecessary due to the bidirectional nature of the design. topology isin when battery is charged to positive Ib. The topology keeps functioning even after the voltage drops to IB 0. Since there is a two-way flow of energy, batteries may be charged and discharged. Fig. 3.4 shows a suggested control flowchart, which is described below.

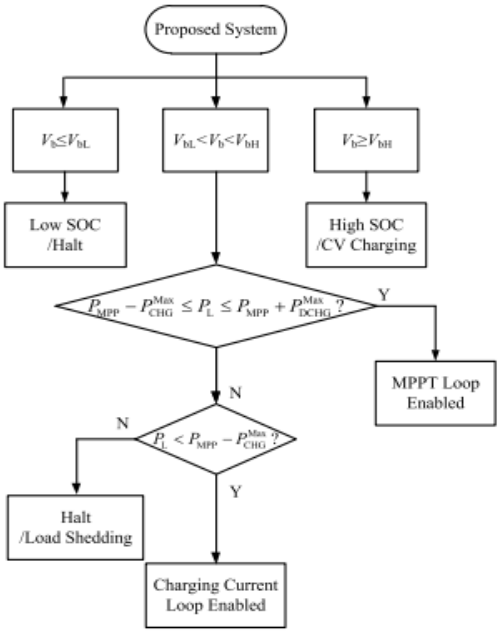

FIGURE 3.4.Flow diagram of the proposed control algorithm.

4. Proposed Three Port Converter fed Induction Motor

In manufacturing, the three-phase machine is the workhorse. Using a motor is the least efficient method of induction, hence this is the one that is most often utilised. Single-phase induction motors are widely used for home appliances and other single-phase applications.

It can be attained by varying the rotor's resistance or by regulating the stator's voltage. However, their low-speed performance is subpar. Changing the supply frequency is the most efficient way to regulate the speed. It's because of this that speeds can vary greatly.

When the machine is not operating at maximum capacity, the ratio v/f stays the same. This maintains a steady power and torque output from the engine. Yet, at lower frequencies, torque decreases, necessitating the use of higher voltage to compensate.

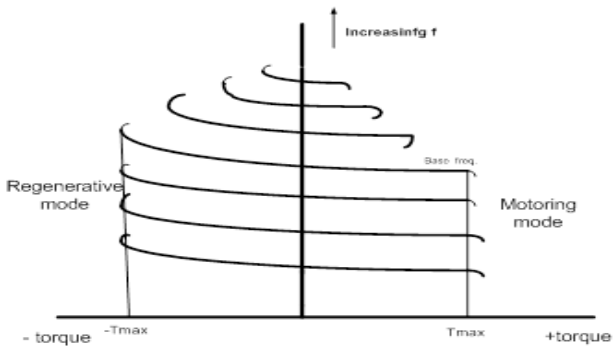

Fig.4.3 (a). Speed Torque Characteristics of Induction Motor with frequency variation

According to the aforementioned graph, the speed may be adjusted and braked anywhere from almost little speed to over synchronous speed.

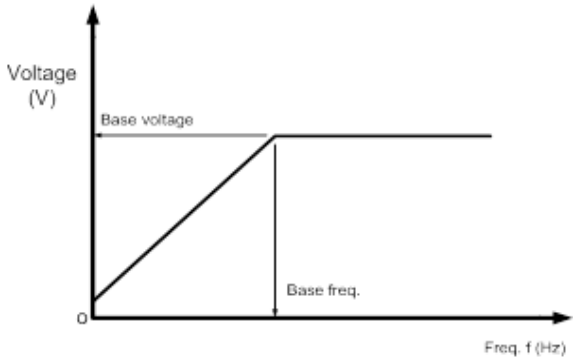

Fig.4.3 (b).voltage and frequency variation in VSI fed Induction motor

It may be demonstrated in Fig.4.3 (b) that V is maintained constant above base speed as freq. rises. Good operating and transient performance may be

achieved with variable frequency management due to the following features:

(a) Both accelerating and decelerating are doable, from rest and beyond the starting velocity.

(b) During transients (starting, braking, and speed reversal), the operation may be carried out at full torque with decreased current, leading to excellent dynamic responsiveness.

Since the operation is carried out at all frequencies between synchronous speed and maximum torque, (c) copper losses are reduced, efficiency and power factor are both maximised, and voltage distortion is avoided.

(c) There is hardly any slowdown while going from a light to a heavy load.

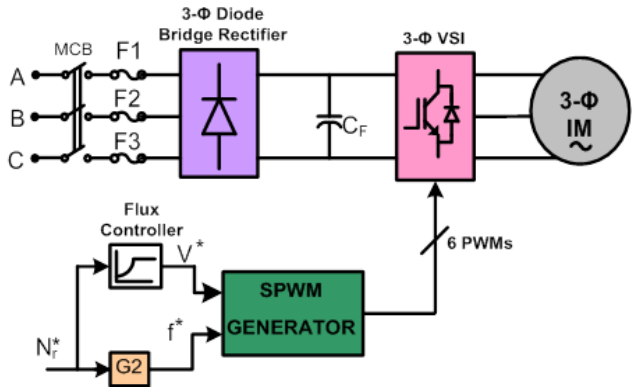

Fig:4.3 (c). Block Diagram Schematic of V/f control of VSI fed 3-phase Induction Motor drive

Fig.4.3 shows a block diagram of a V/f regulated three phase induction motor drive that is supplied by a variable speed inductor (c). To keep the V/f ratio stable, the reference speed input command (Nr*) is used to set the reference frequency (f*) and reference voltage (V*). The 3-phase induction motor is driven by a 3-phase voltage source inverter, which in turn gets reference instructions V* and f* from the SPWM generator.

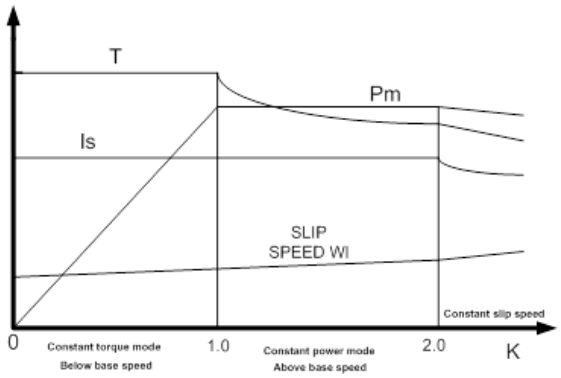

Fig.4.3(d). Modes of operation and variation of is, ωsl,, T and Pm with per unit frequency

5. Simulation Results

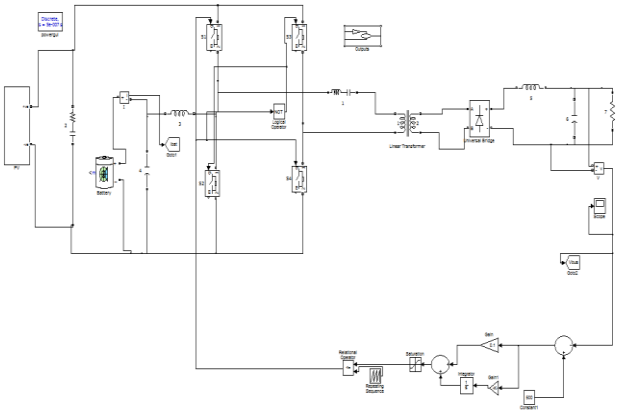

Fig 5.1 Diagram of Proposed System

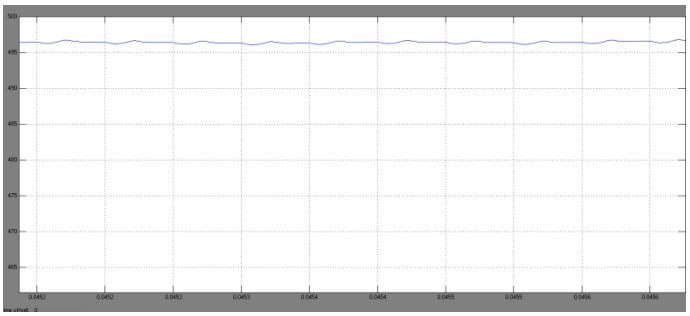

(a) DC bus voltage V bus;

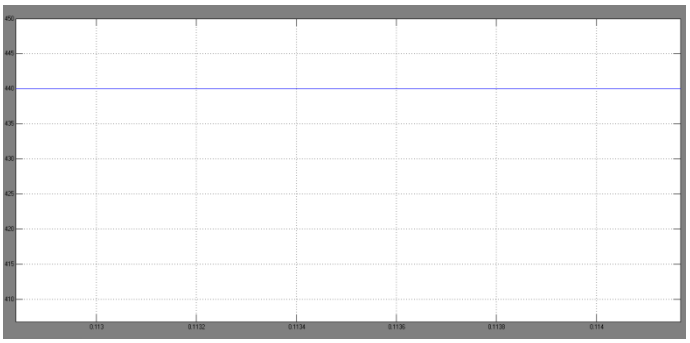

(b) PV voltage VPV;

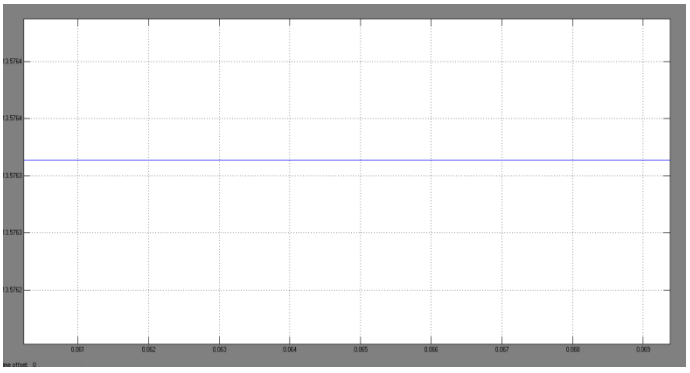

(c) PV current IPV;

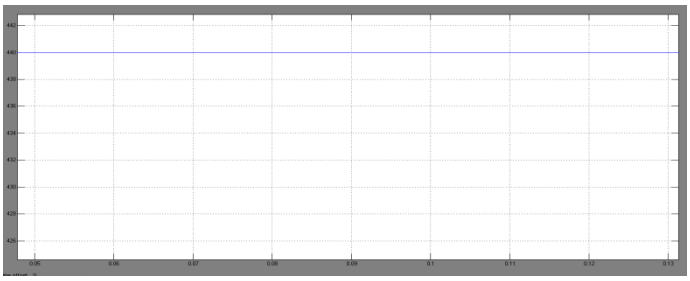

(d) PV reference voltage Vref;

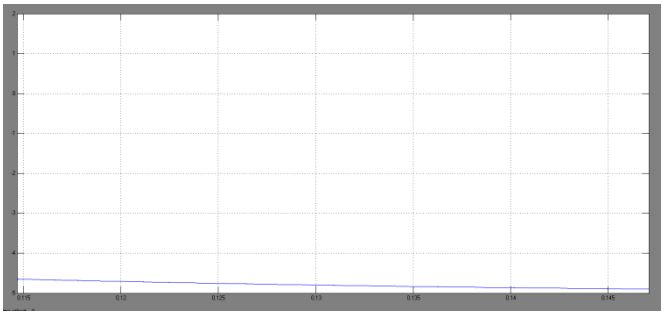

FIGURE 5.2 Steady state simulation results of operation scenario 2. (a) DCbus voltage Vbus; (b) PV voltage VPV; (c) PV current IPV; (d) PV reference voltage Vref; (e) Batter charging current ib.

Figure 5.2 displays the steady-state operating simulation findings. The simulation settings are listed below. The PL D 10 kW load power is determined by using a temperature of 25 degrees Celsius and an irradiance of 1000 W/m2. The 500 V DC bus voltage Vbus is maintained constant by a PI controller regulating the phase shiftangle' (see Fig. 5.2). (a). When the MPPT loop is active, as shown in Fig. 5.2 (b), 5.2 (c), and 5.2 (d), the PV operates at full power, with VPV controlled close to the ideal value VMPP D 435 V and IPV controlled close to the ideal value IMPP D 22 A. (d). Batteries drain and help supply loads, as seen in Fig. 5.2(e).

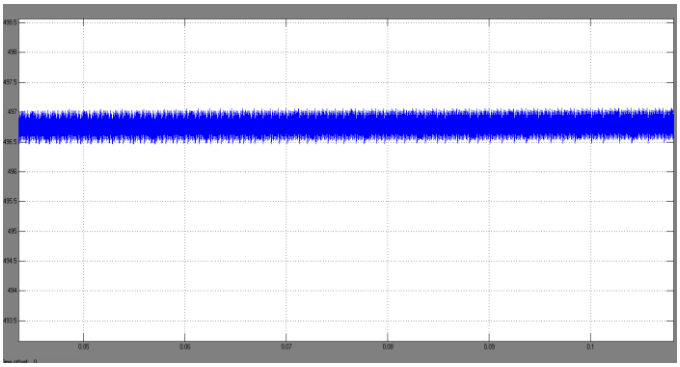

(a) DC bus voltage V bus;

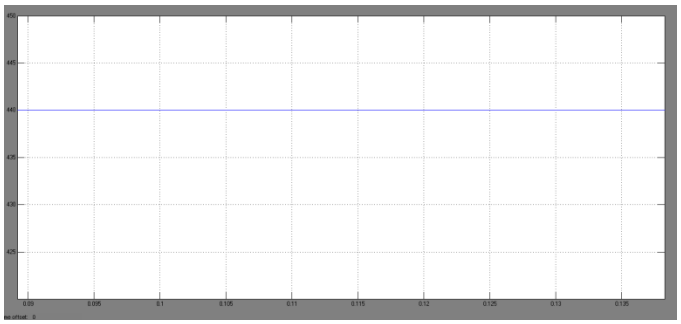

(b) PV voltage VPV;

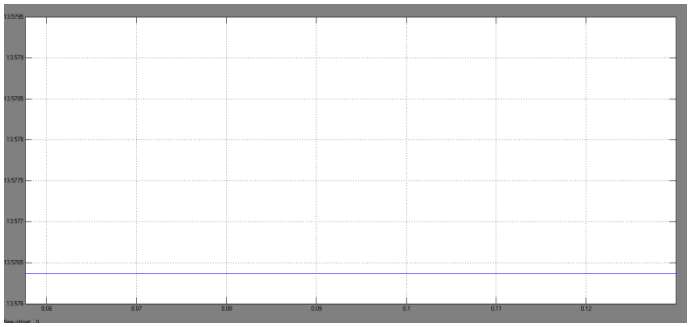

(c) PV current IPV;

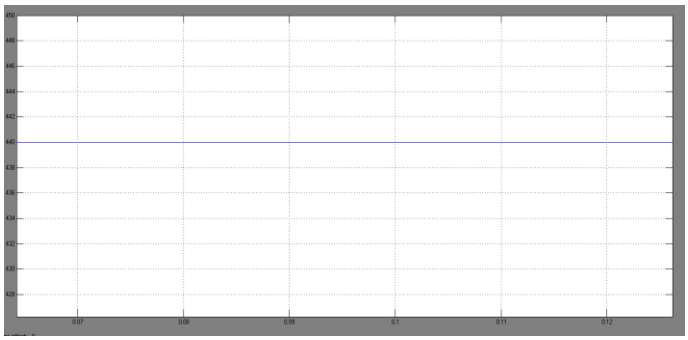

(d) PV reference voltage Vref;

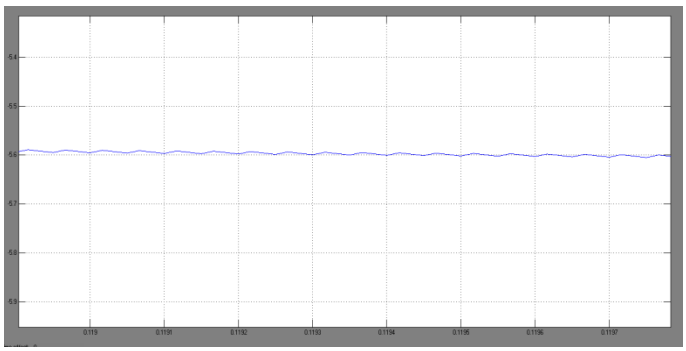

(e) Battery charging current ib.

FIGURE 5.3. Steady state simulation results of operation scenario 4. (a) DCbus voltage Vbus; (b) PV voltage VPV; (c) PV current IPV; (d) PV referencevoltage Vref; (e) Battery charging current ib.

Figure 5.3 displays the outcomes of the simulations in a steady state. The simulation settings are listed below. For the PL D 8 kW load power, we'll use the numbers 25°C, 1000 W/m2, and 50% relative humidity. As can be

seen in Fig. 5.3, the DC bus voltage Vbus is kept constant at 500 Vbus D. (a). With VPV adjusted near the ideal value VMPP D 435 V and IPV controlled near the ideal value IMPP D 22 A, as shown in Fig. 5.3 (b), 5.3 (c), and 5.3 (d), the MPPT loop is allowed and the PV operates at its maximum power point. Power from the PV is being added to the battery, as shown in Fig. 5.3, which is charging (e).

.

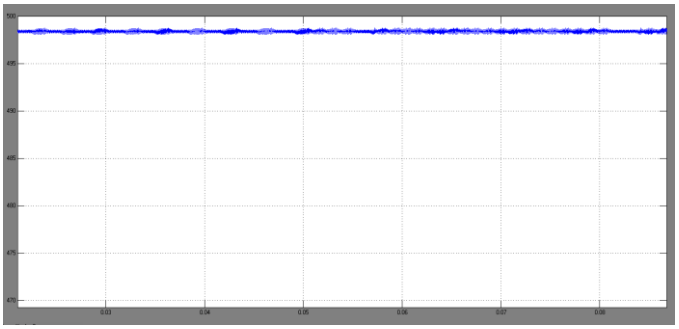

(a)

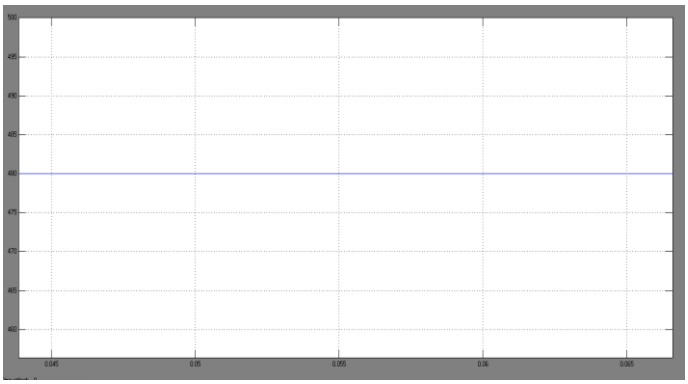

(b)

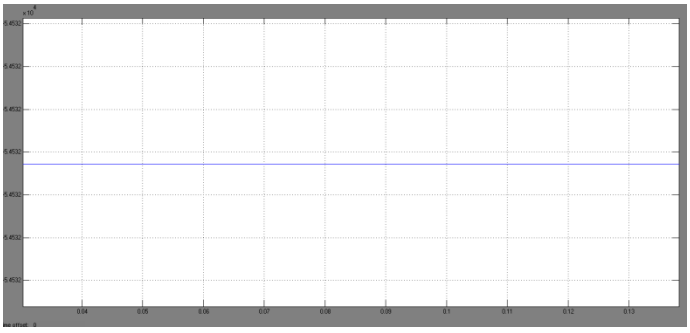

(c)

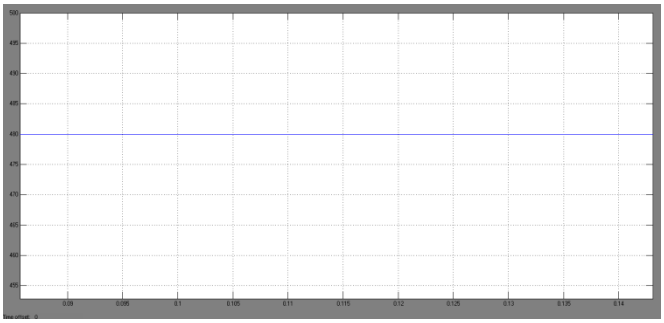

(d)

FIGURE 5.4 The results of scenario 5's steady-state simulation. (a) Voltage from the DC bus Vbus; (b)voltage from the PV modules Vpv; (c)current from the PV modules Ipv; and (d)current from the battery charger ib

In Fig. 5, we see the operation's steady-state outcomes. This is how a simulation works: 1000 W/m2 of radiation, 25 degrees Celsius Figure 5 shows that this value is identical to the one found in Figure 4. (a). In this case, as seen in Fig. 5, the MPPT charger is disabled and the maximum charge current I is set to 30A. (d). According to Figures 5.4 (b) and (c), the PV would not be producing its full potential output under these conditions.

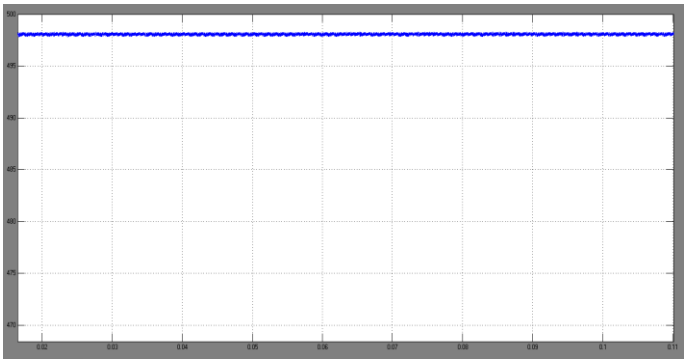

(a)

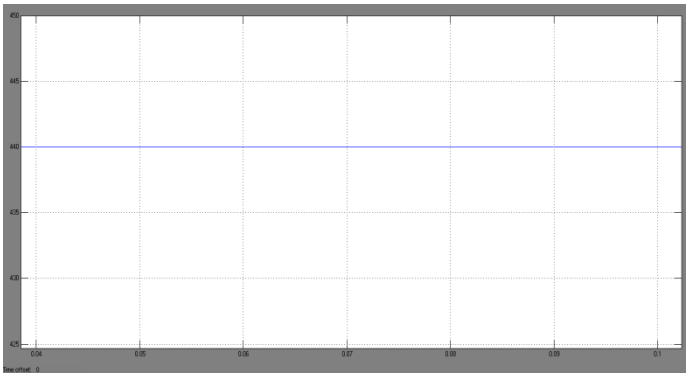

(b)

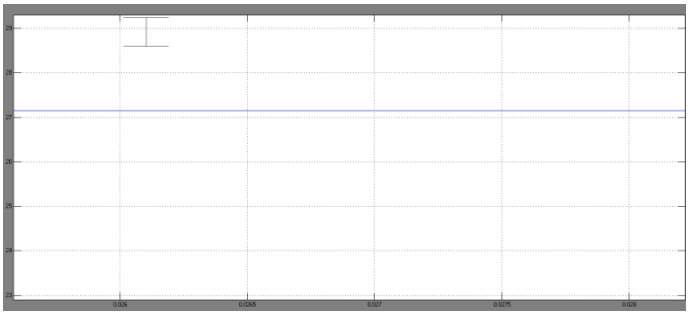

(c)

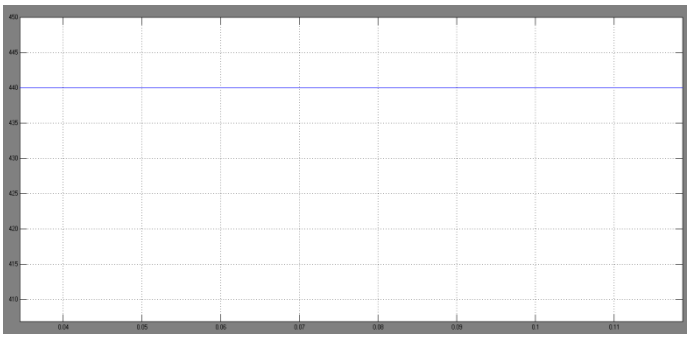

(d)

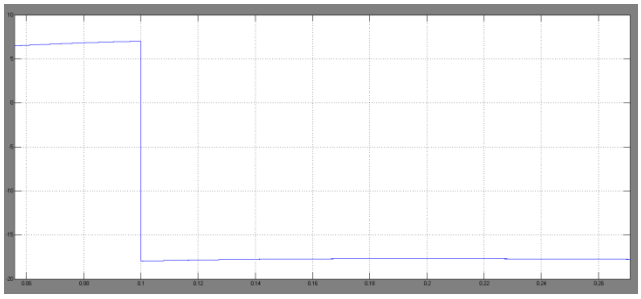

(e)

FIGURE 5.4. The simulation results show that at t = D 2 s, the irradiance drops from 1000 W/m2 to 500 W/m2. (a) Voltage on the DC bus (Vbus); (b)the PV voltage (VPV); (c)the PV current (IPV); (d)the PV reference voltage (Vref); and (e)the battery charging current (ib).

dynamic functionality as seen in Fig. 5, where irradiance is reduced from 1000 W/m2 to 500 W/m2 at time "t" The following are additional rules that may be used in simulations: As can be seen in Fig. 5, the temperature was 25 degrees Celsius, and the load was 8 kilowatts (kW) during the voltage change from bus 4 to bus 5. (a). As seen in Fig. 5, the PV voltage increases whenever the MPPT is in charge of the duty cycle (d) As may be seen in Figures 10(b) and 10(c), MPPT is achieved by running PV close to its maximum power points. Since the battery is shown to be charged before being put to use in Fig. 10 (e), the irradiation incidence may be thought of as a bridge between scenarios 4 and 2.

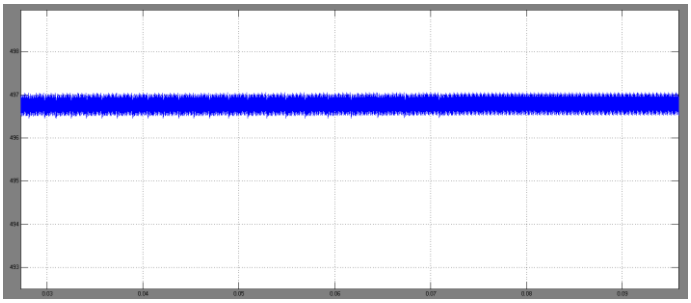

(a)

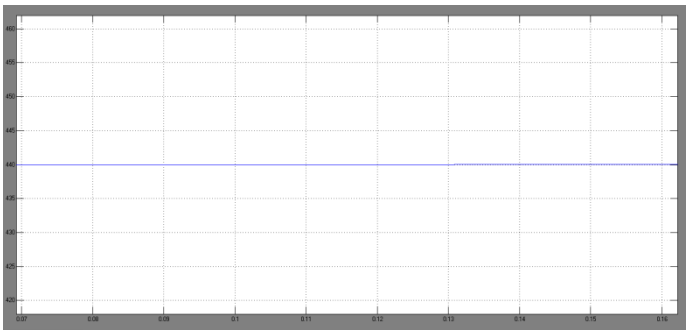

(b)

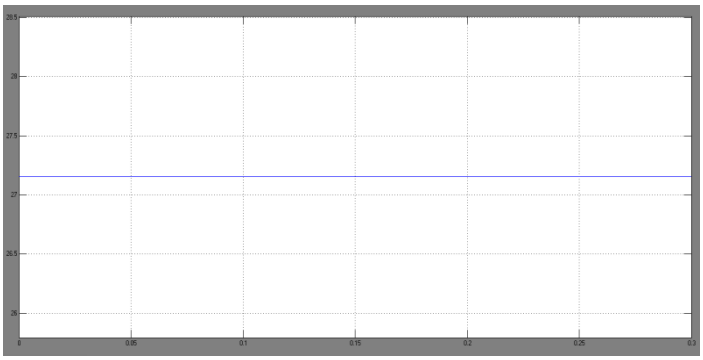

(c)

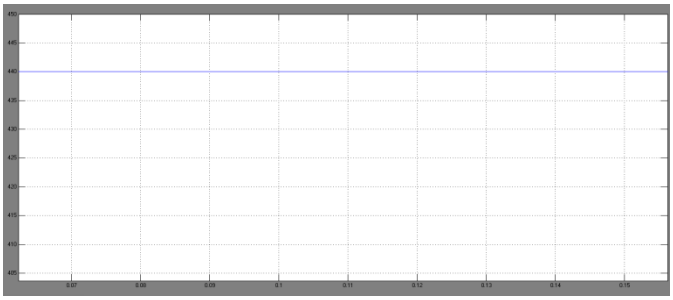

(d)

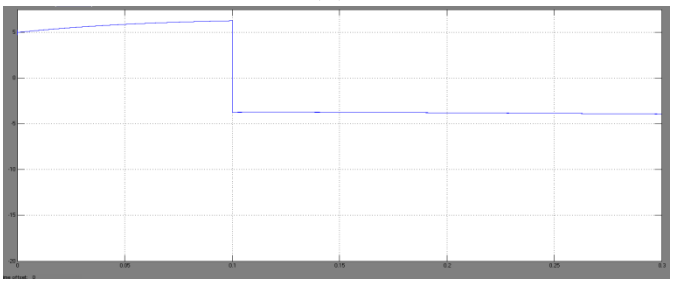

(e)

FIGURE 5.5. Findings from a simulation in which the load power increases from 8 kW to 10 kWat t D 2 s. (a) Voltage on the DC bus (Vbus); (b)the PV voltage (VPV); (c)the PV current (IPV); (d)the PV reference voltage (Vref); and (e)the battery charging current (ib).

Figure 5 depicts the dynamic increase in system output power from 8 kW to 10 kW at time D 2. The following are additional rules that may be used in simulations: (1000 mW/m2 virradiance, 25 °C) The DC bus voltage is shown to be stable in Fig. 5. (a). The original version of Figure 5 has been shortened to just "Figure 5" (d). This

may be seen as the outcome of the load increase shown in Figure 5's Scenario 2 compared to Scenario 5. (e).

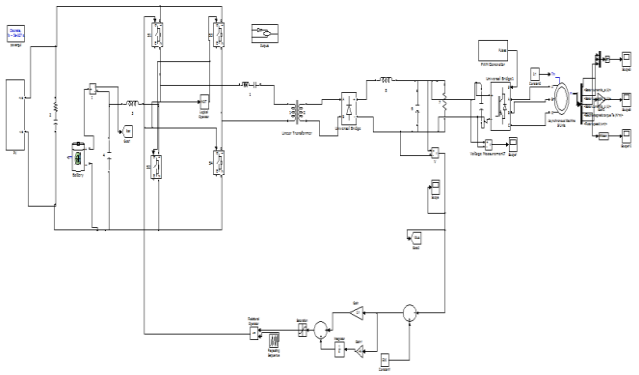

Fig 5.6 A power converter and Induction Motor drive schematic built in Simulink for the proposed system

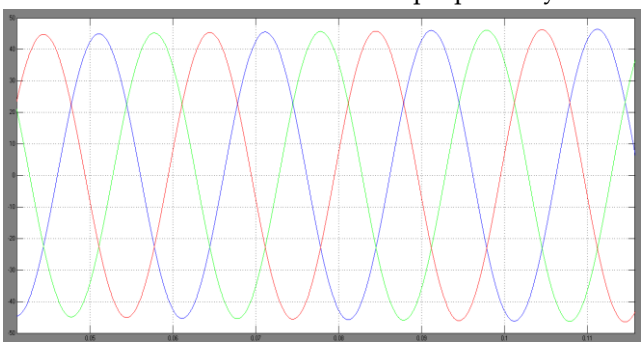

Fig 5.7 The characteristics of the stator current in an Induction motor drive were simulated and shown as waveforms.

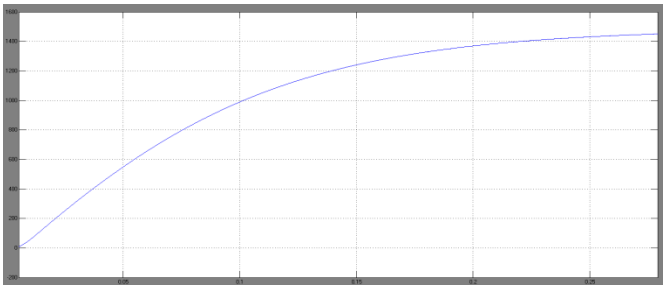

Fig 5.8 Induction motor drive speed characteristics as simulated by waveform simulation

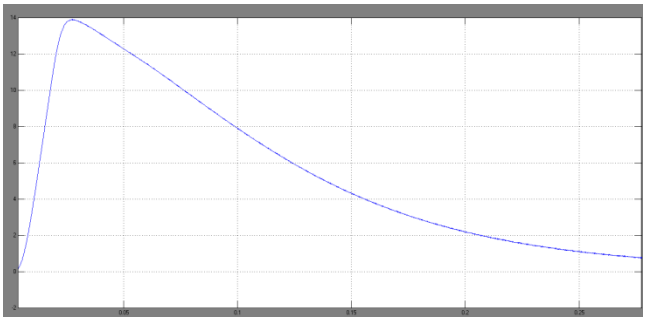

Fig 5.9 Drive waveforms for an simulated induction motor Qualities of Torque

6. Conclusion

A microgrid powered by a renewable hybrid would be an excellent, cost-effective, and environmentally friendly choice. It may be used in lieu of regular gas. In this case, the PV/battery hybrid power generating system incorporates the three-port converter. It fixes the issues with the supply and supplies enough power to run the load. The PV array will be the primary source of electricity for the system when cloud cover and nighttime reduce the amount of sunlight reaching the solar panels. Enhanced power density and/or dependability are two features of the suggested system. To achieve power balance between the three ports, the necessary DC bus voltage is derived from the complete bridge and the switch cycle phase shift angles. In any case, a thorough energy management and control plan is suggested after many different operating situations have been investigated. The priority controller gives you the option to disable the other control loops in order to focus on battery charging and overall system performance.

Conflict of interest statement

Authors declare that they do not have any conflict of interest.

References

[1] F. Blaabjerg, Z. Chen, and S. B. Kjaer, ‘‘Power electronics as efficientinterface in dispersed power generation systems,’’ IEEE Trans. PowerElectron., vol. 19, no. 5, pp. 1184–1194, Sep. 2004.

[2] J. M. Carrasco, L. G. Franquelo, J. T. Bialasiewicz, E. Galvan, R. Potillo,M. M. Prats, J. I. Leon, and N. Moreno-Alfonso, ‘‘Power-electronic systems for the grid integration of renewable energy sources: A survey,’’ IEEETrans. Ind. Electron., vol. 53, no. 4, pp. 1002–1016, Jun. 2006.

[3] BP Statistical Review of World Energy, British Petroleum, London, U.K.,Jun. 2018.

[4] J. P. Barton and D. G. Infield, ‘‘Energy storage and its use with intermittent renewable energy,’’ IEEE Trans. Energy Convers., vol. 19, no. 2,pp. 441–448, Jun. 2004.

[5] M. S. Whittingham, ‘‘History, evolution, and future status of energy storage,’’ Proc. IEEE, vol. 100, pp. 1518–1534, May 2012.

[6] C. A. Hill, M. C. Such, D. Chen, J. Gonzalez, and W. M. Grady, ‘‘Batteryenergy storage for enabling integration of distributed solar power generation,’’ IEEE Trans. Smart Grid, vol. 3, no. 2, pp. 850–857, Jun. 2012.

[7] Z. Yi, W. Dong, and A. H. Etemadi, ''A unified control and power management scheme for PV-battery-based hybrid microgrids for both gridconnected and islanded modes,'' IEEE Trans. Smart Grid, vol. 9, no. 6,pp. 5975–5985, Nov. 2018.

[8] H. Mahmood, D. Michaelson, and J. Jiang, ''Decentralized power management of a PV/battery hybrid unit in a droop-controlled islanded microgrid,''IEEE Trans. Power Electron., vol. 30, no. 12, pp. 7215–7229, Dec. 2015.

[9] K. Sun, L. Zhang, Y. Xing, and J. M. Guerrero, ''A distributed controlstrategy based on DC bus signaling for modular photovoltaic generation systems with battery energy storage,'' IEEE Trans. Power Electron.,vol. 26, no. 10, pp. 3032–3045, Oct. 2011.

[10] S. Adhikari and F. Li, ''Coordinated V-f and P-Q control of solar photovoltaic generators with MPPT and battery storage in microgrids,'' IEEETrans. Smart Grid, vol. 5, no. 3, pp. 1270–1281, May 2014.

[11] S. K. Kollimalla, M. K. Mishra, and N. L. Narasamma, ''Design and analysis of novel control strategy for battery and supercapacitor storage system,''IEEE Trans. Sustain. Energy, vol. 5, no. 4, pp. 1137–1144, Oct. 2014.

[12] S. Wen, S. Wang, G. Liu, and R. Liu, ''Energy management and coordinated control strategy of PV/HESS AC microgrid during Islanded operation,'' IEEE Access, vol. 7, pp. 4432–4441, 2019.

[13] W. Jiang and B. Fahimi, ''Multiport power electronic interface—Concept,modeling, and design,'' IEEE Trans. Power Electron., vol. 26, no. 7,pp. 1890–1900, Jul. 2011.

[14] H. Krishnaswami and N. Mohan, ''Three-port series-resonant DC–DCconverter to interface renewable energy sources with bidirectional loadand energy storage ports,'' IEEE Trans. Power Electron., vol. 24, no. 10,pp. 2289–2297, Oct. 2009.

[15] H. Tao, J. L. Duarte, and M. A. M. Hendrix, ''Three-port triple-half-bridgebidirectional converter with zero-voltage switching,'' IEEE Trans. PowerElectron., vol. 23, no. 2, pp. 782–792, Mar. 2008.

[16] Z. Qian, O. Abdel-Rahman, and I. Batarseh, ''An integrated four-portDC/DC converter for renewable energy applications,'' IEEE Trans. PowerElectron., vol. 25, no. 7, pp. 1877–1887, Jul. 2010.

[17] H. Al-Atrash and I. Batarseh, ''Boost-integrated phase-shift full-bridgeconverter for three-port interface,'' in Proc. IEEE Power Electron. Spec.Conf., Jun. 2007, pp. 2313–2321.

[18] W. Li, J. Xiao, Y. Zhao, and X. He, ''PWM plus phase angle shift (PPAS)control scheme for combined multiport DC/DC converters,'' IEEE Trans.Power Electron., vol. 27, no. 3, pp. 1479–1489, Mar. 2012.

[19] T. Esram and P. L. Chapman, ''Comparison of photovoltaic array maximumpower point tracking techniques,'' IEEE Trans. Energy Convers., vol. 22,no. 2, pp. 439–449, Jun. 2007.